

ON THE PERFORMANCE OF THE VARIATIONAL MULTISCALE FORMULATION FOR SUBSURFACE FLOW AND TRANSPORT IN HETEROGENEOUS POROUS MEDIA

D. Z. TURNER, K. B. NAKSHATRALA, AND P. K. NOTZ

ABSTRACT. The following work compares two popular mixed finite elements used to model subsurface flow and transport in heterogeneous porous media; the lowest order Raviart-Thomas element and the variational multiscale stabilized element. Comparison is made based on performance for several problems of engineering relevance that involve highly heterogeneous material properties (permeability ratios of up to 1×10^5), open flow boundary conditions (pressure driven flows), and large scale domains in two dimensions. Numerical experiments are performed to show the degree to which mass conservation is violated when a flow field computed using either element is used as the advection velocity in a transport model. The results reveal that the variational multiscale element shows considerable mass production or loss for problems that involve flow tangential to layers of differing permeability, but marginal violation of local mass balance for problems of less orthogonality in the permeability. The results are useful in establishing rudimentary estimates of the error produced by using the variational multiscale element for several different types of problems.

1. INTRODUCTION

In the field of subsurface modeling, choosing the right numerical formulation for a particular problem of interest can be a difficult choice. There are a number of trade-offs that one must consider. Two very important considerations involve accuracy and computational efficiency. For problems that involve species transport (reactive or not) through a porous domain, artificial production or loss of constituents can be detrimental, especially in the case of transport of contaminants or pollutants. At the same time, accuracy comes with a cost, which manifests in the form of computation time, mesh resolution requirements, and/or time step restrictions. An astute analyst must balance these tradeoffs such that sufficiently accurate results are obtained at a reasonable cost.

In this paper, we compare two popular mixed finite element formulations to solve the flow equations in heterogeneous porous media. The two mixed formulations are the lowest order Raviart-Thomas formulation (RT0) [1], and the variational multiscale stabilized formulation (VMS), which

Date: October 31, 2018.

Key words and phrases. flow through porous media; local mass balance; spatial heterogeneity; variational multiscale formulation; Raviart-Thomas spaces; mixed finite element formulations.

Corresponding author: Daniel Z. Turner, e-mail: dzturne@sandia.gov, phone: +1-(505)-845-0268.

has been studied in references [2, 3, 4, 5]. Mixed methods, that treat velocity and pressure as independent variables, as opposed to single field formulations, provide a more accurate representation of the velocity field, but are susceptible to instability engendered by the saddle-point nature of the system of equations [6]. The VMS element evaluated in this work consists of equal order linear interpolation of the velocity and pressure fields, for which the degrees of freedom live at the node locations. The VMS element achieves stability through the addition of residual based terms to the formulation such that the LBB condition is circumvented. The lowest order Raviart-Thomas finite element formulation (RT0) consists of evaluating fluxes over the midpoint of element edges and constant pressures within the element and is based on an LBB stable finite element space. A schematic of both elements is presented in Figure 1. Both elements are used to solve several realistic engineering problems involving flow and transport in heterogeneous porous media.

The pursuit of stable, locally conservative finite element formulations has received substantial attention (for examples see [7, 8, 9] among many others). In addition, a number of comparisons have been made between various formulations (for example, see [10, 11, 12]), Of particular interest is the work presented in [12] that showed a computational efficiency advantage for control volume approaches vs. mixed methods for problems with only moderate heterogeneity.

It is well known that the VMS element, which is based on a Galerkin formulation is not locally mass conserving (without additional sophistication being built into the algorithm as in [13, 14]), but the degree to which a realistic simulation will suffer due to this shortcoming of the VMS element is not well documented. Additionally, although the RT0 element is locally conservative, it has only been shown viable for triangular or tetrahedral elements (quadrilateral variants of this method do not pass the patch test). In the context of heterogeneous materials, this work aims, to evaluate the strengths and weaknesses of either approach for problems with highly varying material permeability and predominantly open flow boundary conditions. The results have applications in subsurface simulations for which the far-field boundary is typically described with some type of pressure boundary condition.

1.1. Main contributions of this paper. One of the main goals of this paper is to assess the performance of the variational multiscale formulation with respect to local (or element) mass balance using a coupled flow-transport model. The assessment is performed by comparing the variational multiscale formulation with the lowest-order Raviart-Thomas formulation, which possesses the local mass balance property. We also take into account the dependence of viscosity on the pressure, which is the case with most organic liquids and supercritical carbon-dioxide. Using Barus model (in which the viscosity varies exponentially with respect to pressure), we study the affect of the dependence of viscosity of pressure on the error in the local mass balance under the variational

multiscale formulation. Using canonical problems, we also compare the performance of the variational multiscale formulation and the lowest order Raviart-Thomas formulation with respect to memory storage, time for assembling matrices, and total CPU time.

1.2. Organization of the paper. The remainder of this paper is organized as follows. In Section 2, we present a coupled flow-transport mathematical model. In Section 3, we present weak formulations to solve both flow and transport problems. For the flow problem, we consider the variational multiscale formulation and the lowest-order Raviart-Thomas formulation. In Section 4, we present numerical results for flow and transport for three canonical problems: a stratified set of layers with differing permeabilities, a cylindrical inclusion of high permeability in a domain of lower permeability, and a leaky well scenario where a storage aquifer leaks the injected constituent through an abandoned well. In Section 5, we conclude with a summary of the important research findings of this paper.

2. A COUPLED FLOW-TRANSPORT MATHEMATICAL MODEL

Consider the transport of a chemical species in a rigid porous medium (that is, the deformation of the porous solid is neglected). We shall assume that the porous medium is fully saturated with a (moving) fluid. Herein, we consider modified Darcy equation for the flow problem which (as the name suggests) is a modification to the standard Darcy equation [15]. This model takes into account the dependence of viscosity on the pressure. The fluid is still assumed to be incompressible. The transport model consists of transient advection-diffusion equation wherein the advection velocity is given by the flow problem.

2.1. Governing equations for the flow problem. Let Ω be a bounded open domain, and Γ be its piecewise smooth boundary ($\Gamma := \bar{\Omega} - \Omega$, where $\bar{\Omega}$ is the set closure of Ω). A spatial point is denoted by $\mathbf{x} \in \Omega$. The gradient and divergence operators with respect to \mathbf{x} are, respectively, denoted by $\text{grad}[\cdot]$ and $\text{div}[\cdot]$. Let $p : \Omega \rightarrow \mathbb{R}$ denote the pressure, and the velocity field is denoted by $\mathbf{v} : \Omega \rightarrow \mathbb{R}^{nd}$, where “ nd ” is the number of spatial dimensions. We denote the density by ρ , the permeability by $k(\mathbf{x})$, and the coefficient of viscosity by μ . We consider the following expressions for the dependence of viscosity on the pressure:

$$\mu(p) = \mu_0 \tag{1a}$$

$$\mu(p) = \mu_0 \exp[\beta p] \tag{1b}$$

where $\mu_0 > 0$ is the coefficient of viscosity at a reference pressure (e.g., at the atmospheric pressure), and $\beta \geq 0$ is a constant. Equation (1a) assumes the viscosity is constant, which is the case in the standard Darcy flow model [15]. Equation (1b) is commonly referred to as Barus formula [16].

We write the governing equations for the flow in first-order form (or mixed form) in which the velocity and pressure are treated as independent variables. The governing equations for the flow problem can be written as follows:

$$\frac{\mu(p)}{k} \mathbf{v} + \text{grad}[p] = \rho \mathbf{b}(\mathbf{x}) \quad \text{in } \Omega \quad (2a)$$

$$\text{div}[\mathbf{v}] = \phi(\mathbf{x}) \quad \text{in } \Omega \quad (2b)$$

$$\mathbf{v}(\mathbf{x}) \cdot \mathbf{n}(\mathbf{x}) = \psi(\mathbf{x}) \quad \text{on } \Gamma \quad (2c)$$

where $\mathbf{b}(\mathbf{x})$ is the specific body force, $\phi(\mathbf{x})$ is the prescribed volumetric flow rate, $\psi(\mathbf{x})$ is the prescribed normal component of the velocity on the boundary, and $\mathbf{n}(\mathbf{x})$ is the unit outward normal vector to Γ . Note that for a given Ω (and hence for a given Γ), $\phi(\mathbf{x})$ and $\psi(\mathbf{x})$ are not independent of each other, and they need to satisfy the following compatibility condition:

$$\int_{\Omega} \phi(\mathbf{x}) \, d\Omega = \int_{\Gamma} \psi(\mathbf{x}) \, d\Gamma \quad (3)$$

Since we have prescribed only the normal component of the velocity on the whole boundary, one need to enforce one more condition to obtain unique solution in the pressure field. This is typically achieved by meeting the following condition:

$$\int_{\Omega} p(\mathbf{x}) \, d\Omega = 0 \quad (4)$$

Another way to achieve uniqueness in the pressure field is to prescribe the pressure at a point to fix the datum, which is computationally the most convenient and is employed in this paper. In pressure-driven flows, there is no need to enforce additional conditions for uniqueness as the pressure is prescribed on a set of non-zero measure on the boundary.

2.2. Governing equations for the transport problem. Let $c(\mathbf{x}, t)$ denote the concentration, and \mathcal{I} denote the time interval of interest. The boundary Γ is divided into two complementary parts Γ_c^D and Γ_c^N . Γ_c^D is that part of the boundary on which Dirichlet boundary condition is prescribed (that is, the concentration is prescribed), and Γ_c^N is that part of the boundary on which the Neumann boundary condition is prescribed. The transport problem is to find $c(\mathbf{x}, t)$ by solving the following initial boundary value problem:

$$\frac{\partial c}{\partial t} + \mathbf{v}(\mathbf{x}) \cdot \text{grad}[c] - \text{div}[D \text{grad}[c]] = f(\mathbf{x}, t) \quad \text{in } \Omega \times \mathcal{I} \quad (5a)$$

$$c(\mathbf{x}, t) = c^P(\mathbf{x}, t) \quad \text{on } \Gamma_c^D \times \mathcal{I} \quad (5b)$$

$$D \text{grad}[c] \cdot \mathbf{n}(\mathbf{x}) = t^P(\mathbf{x}, t) \quad \text{on } \Gamma_c^N \times \mathcal{I} \quad (5c)$$

where D is the constant diffusivity of the species, $c^P(\mathbf{x}, t)$ is the prescribed Dirichlet boundary condition on concentration, $t^P(\mathbf{x}, t)$ is the prescribed flux, $f(\mathbf{x}, t)$ is the volumetric source term, and $\mathbf{n}(\mathbf{x})$ is the unit outward normal vector to Γ .

3. WEAK FORMULATIONS

In this section, we present two mixed formulations for the flow problem, and a single-field formulation for solving the transport problem. The first mixed formulation is based on the Raviart-Thomas spaces, and the other is the variational multiscale formulation presented in Reference [5].

3.1. Weak mixed formulations for the flow problem. Let the weighting function corresponding to the velocity be denoted by $\mathbf{w}(\mathbf{x})$, and the weighting function corresponding to the pressure be denoted by $q(\mathbf{x})$. The relevant function spaces for the velocity and the corresponding weighting function are, respectively, defined as follows:

$$\mathcal{V} := \{\mathbf{v}(\mathbf{x}) | \mathbf{v}(\mathbf{x}) \in (L_2(\Omega))^{nd}, \operatorname{div}[\mathbf{v}] \in L_2(\Omega), \operatorname{trace}[\mathbf{v} \cdot \mathbf{n}] = \psi(\mathbf{x}) \in H^{-1/2}(\Gamma)\} \quad (6a)$$

$$\mathcal{W} := \{\mathbf{w}(\mathbf{x}) | \mathbf{w}(\mathbf{x}) \in (L_2(\Omega))^{nd}, \operatorname{div}[\mathbf{w}] \in L_2(\Omega), \operatorname{trace}[\mathbf{w} \cdot \mathbf{n}] = 0 \text{ on } \Gamma\} \quad (6b)$$

where $L_2(\Omega)$ is the space of square integrable functions, $\operatorname{trace}[\cdot]$ is the standard trace operator used in functional analysis [17], and $H^{-1/2}(\Gamma)$ is the dual space of $H^{1/2}(\Gamma)$. In the classical mixed formulation, the function space for the pressure and its corresponding weighting function is defined as follows:

$$\mathcal{P} := \{p(\mathbf{x}) | p(\mathbf{x}) \in L_2(\Omega), \int_{\Omega} p(\mathbf{x}) \, d\Omega = 0\} \quad (7)$$

In the variational multiscale formulation, the function space for the pressure and its corresponding weighting function is defined as follows:

$$\bar{\mathcal{P}} := \{p(\mathbf{x}) | p(\mathbf{x}) \in H^1(\Omega), \int_{\Omega} p(\mathbf{x}) \, d\Omega = 0\} \quad (8)$$

where $H^1(\Omega)$ is a standard Sobolev space [18]. We shall employ the following notation for the standard L^2 inner product:

$$(\mathbf{a}; \mathbf{b}) = \int_{\Omega} \mathbf{a} \cdot \mathbf{b} \, d\Omega \quad (9)$$

3.1.1. Classical mixed formulation and Raviart-Thomas spaces. The classical mixed formulation reads: Find $\mathbf{v}(\mathbf{x}) \in \mathcal{V}$ and $p(\mathbf{x}) \in \mathcal{P}$ such that we have

$$\left(\mathbf{w}; \frac{\mu}{k} \mathbf{v}\right) - (\operatorname{div}[\mathbf{v}]; p) - (q; \operatorname{div}[\mathbf{v}] - \phi) = (\mathbf{w}; \rho \mathbf{b}) \quad \forall \mathbf{w}(\mathbf{x}) \in \mathcal{W}, q(\mathbf{x}) \in \mathcal{P} \quad (10)$$

Let \mathcal{V}_h , \mathcal{W}_h and \mathcal{P}_h are, respectively, appropriate subspaces of \mathcal{V} , \mathcal{W} and \mathcal{P} . A (conforming) finite element formulation reads: Find $\mathbf{v}_h(\mathbf{x}) \in \mathcal{V}_h$ and $p_h(\mathbf{x}) \in \mathcal{P}_h$ such that we have

$$\left(\mathbf{w}_h; \frac{\mu}{k} \mathbf{v}_h\right) - (\operatorname{div}[\mathbf{v}_h]; p_h) - (q_h; \operatorname{div}[\mathbf{v}_h] - \phi) = (\mathbf{w}_h; \rho \mathbf{b}) \quad \forall \mathbf{w}_h(\mathbf{x}) \in \mathcal{W}_h, q_h(\mathbf{x}) \in \mathcal{P}_h \quad (11)$$

It is well-known that inclusions $\mathcal{V}_h \subset \mathcal{V}$, $\mathcal{W}_h \subset \mathcal{W}$ and $\mathcal{P}_h \subset \mathcal{P}$ do not insure stable numerical results. Specifically, not all combinations of interpolation functions for the velocity and pressure are stable.

A mathematical theory concerning the stability of formulations and choice of appropriate finite dimensional spaces is given by Ladyzhenskaya-Babuška-Brezzi (LBB) stability condition [19, 20, 18].

In the literature one can find two different ways of obtaining stable results: circumventing the LBB condition and satisfying the LBB condition [21]. In the former category, stabilization terms are added to the classical mixed formulation to achieve stability. Many stabilized formulations fall in the former category (e.g., references [22, 23, 5]). Some of the approaches in the later category are Raviart-Thomas spaces [1], Brezzi-Douglas-Marini spaces [24]. In this paper, for the flow problem, we shall consider the lowest order Raviart-Thomas spaces and the variational multiscale formulation.

We now present the lowest-order Raviart-Thomas triangular spaces. Let \mathcal{T}_h be triangulation on Ω . The lowest order finite dimensional subspaces on triangles are defined as follows:

$$\mathcal{V}_h := \{\mathbf{v} = (v^{(1)}, v^{(2)}) \mid v_K^{(1)} = a_K + b_K x, v_K^{(2)} = c_K + b_K y; a_K, b_K, c_K \in \mathbb{R}; K \in \mathcal{T}_h\} \quad (12a)$$

$$\mathcal{W}_h := \{\mathbf{w} = (w^{(1)}, w^{(2)}) \mid w_K^{(1)} = a_K + b_K x, w_K^{(2)} = c_K + b_K y; a_K, b_K, c_K \in \mathbb{R}; K \in \mathcal{T}_h\} \quad (12b)$$

$$\mathcal{P}_h := \{p(\mathbf{x}) \mid p(\mathbf{x}) = \text{a constant on each triangle } K \in \mathcal{T}_h\} \quad (12c)$$

3.1.2. *Variational multiscale formulation.* A stabilized formulation based on the variational multiscale formalism can be written as follows [4]: Find $\mathbf{v}(\mathbf{x}) \in \mathcal{V}$ and $p(\mathbf{x}) \in \mathcal{Q}$ such that we have

$$\begin{aligned} (\mathbf{w}; \frac{\mu}{k} \mathbf{v}) - (\text{div}[\mathbf{w}]; p) - (q; \text{div}[\mathbf{v}] - \phi) - (\mathbf{w}; \rho \mathbf{b}) \\ - \frac{1}{2} \left(\frac{\mu}{k} \mathbf{w} + \text{grad}[q]; \frac{k}{\mu} (\frac{\mu}{k} \mathbf{v} + \text{grad}[p] - \rho \mathbf{b}) \right) = 0 \quad \forall \mathbf{w}(\mathbf{x}) \in \mathcal{W}, q(\mathbf{x}) \in \mathcal{Q} \end{aligned} \quad (13)$$

Remark 1. *If the coefficient of viscosity is constant the formulation presented in Reference [4] is same as the formulation discussed in References [22, 23].*

3.1.3. *Pressure boundary conditions.* It is well-known that strongly enforced outflow boundary conditions can produce spurious oscillations in the solution [25, 26, 27, 28]. Let Γ_p denote that part of the boundary on which the pressure is prescribed, and let Γ_v be that part of the boundary on which the normal component of the velocity is prescribed. (As usual, for well-posedness we have $\Gamma_v \cup \Gamma_p = \Gamma$ and $\Gamma_v \cap \Gamma_p = \emptyset$.) A simple procedure for enforcing the pressure boundary condition is to replace the term $-(\text{div}[\mathbf{w}]; p)$ with the terms

$$-(\text{div}[\mathbf{w}; p] + (\mathbf{w} \cdot \mathbf{n}; p_0)_{\Gamma_p})$$

in the mathematical statements (10) and (13) and subsequent steps. In such cases, the function spaces for the velocity and corresponding weighting function will be modified as follows:

$$\mathcal{V} := \{\mathbf{v}(\mathbf{x}) \mid \mathbf{v}(\mathbf{x}) \in (L_2(\Omega))^{nd}, \text{div}[\mathbf{v}] \in L_2(\Omega), \text{trace}[\mathbf{v} \cdot \mathbf{n}] = \psi(\mathbf{x}) \in H^{-1/2}(\Gamma_v)\}$$

$$\mathcal{W} := \{\mathbf{w}(\mathbf{x}) \mid \mathbf{w}(\mathbf{x}) \in (L_2(\Omega))^{nd}, \text{div}[\mathbf{w}] \in L_2(\Omega), \text{trace}[\mathbf{w} \cdot \mathbf{n}] = 0 \text{ on } \Gamma_v\}$$

TABLE 1. Summary of formulation properties

	Global	Local (element)	Convergence	Convergence
Formulation	mass balance	mass balance	rate velocity	rate pressure
RT0	Yes	Yes	1.0	1.0
VMS	Yes	No	2.0	1.0

3.2. Weak formulation for the transport problem. We employ the standard single-field formulation to solve the transport equations, which is based on the Galerkin principle. Let us denote the weighting function corresponding to the concentration as $w^c(\mathbf{x})$. We shall define the following function spaces for the concentration and the corresponding weighting function:

$$\mathcal{C}_t := \{c(\mathbf{x}, t) \mid c(\mathbf{x}, t) \in H^1(\Omega), c(\mathbf{x}, t) = c^p(\mathbf{x}, t) \text{ on } \Gamma_c^D\} \quad (14a)$$

$$\mathcal{W}^c := \{w^c(\mathbf{x}) \mid w^c(\mathbf{x}) \in H^1(\Omega), w^c(\mathbf{x}) = 0 \text{ on } \Gamma_c^D\} \quad (14b)$$

The weak form can be expressed as: Find $c(\mathbf{x}, t) \in \mathcal{C}_t$ such that

$$(w; \frac{\partial c}{\partial t}) + (w^c; \mathbf{v} \cdot \text{grad}[c]) + (\text{grad}[w^c]; D \text{grad}[c]) = (w^c; f) + (w^c; t^p)_{\Gamma_c^D} \quad \forall w^c(\mathbf{x}) \in \mathcal{W}^c \quad (15)$$

Remark 2. *In addition to the local mass balance error associated with the flow problem, there will also be an error associated with the transport problem. Since the focus of this work is on the characteristics of the flow problem we are assuming that the transport error is the same for the velocity field generated by both the RT0 and VMS formulations.*

4. REPRESENTATIVE NUMERICAL RESULTS

In the following section we present results from three numerical examples involving flow and transport in porous domains with heterogeneous material properties. For all examples, the mesh was constructed from linear triangular elements. Identical meshes were used for both the RT0 and VMS elements. A direct solver (Amesos umfpack [29]) was used to solve the resulting system of equations in serial on a desktop machine, using an Intel Xeon CPU (2.93 GHz). For all examples, a constant species diffusivity, $D = 0.01$ was used. Also, the Backward Euler method was used for time integration with a time step, $\Delta t = 0.01$ s, and the residual tolerance was set to 1×10^{-9} .

4.1. Multilayer problem. For the multilayer problem (which is a modification of an example given in [30, 31]), the unit square domain $\Omega = (0, 1) \times (0, 1)$, shown in Figure 2, is divided into five layers of thickness 0.2 units, each with a unique ratio, k/μ . Within each layer, the ratio is constant, but changes as a step function at the layer boundaries. The flow is driven by a pressure difference prescribed on the left and right boundary of the domain. The properties used for this problem are defined in Table 2. The computational mesh used for the multilayer problem is shown in Figure 2.

The exact solution for the pressure is a linear drop across the domain. The exact solution for the velocity in each layer is equal to the ratio, k/μ . Figure 3 shows the x -velocity along the centerline of the domain taken at $x = 0.5$. Note from the figure that the RT0 element captures the exact solution for the velocity in each layer and the jump in velocity between layers. The VMS element is not able to accurately capture the jump in velocity between layers. This is due to the well-known property that a continuous element will enforce continuity of the velocity in both the normal and tangential directions, although discontinuity in the tangential direction is physically realizable. Ironically (for a *stabilized* method), in addition to smoothing the velocity in the vicinity of permeability jumps, the VMS element shows oscillations in the velocity within each layer. It can be shown that with increasing disparity between layer properties, these oscillations increase in magnitude.

Figures 4, 5, and 6 show the results of using the computed velocity field as the advection velocity for the transport problem defined by equation (5a). In this case, the problem represents transport of a species through a stratified system of permeabilities. Along the left edge of the domain, the concentration is held constant in time at 1.0. As time progresses, the species advects and diffuses through the domain at different rates, given the local flow velocity with each layer. Even though the VMS element shows significant overshoots and undershoots for the velocity in the vicinity of the permeability jumps, the two elements show close correlation in terms of concentration of the species in time. Figure 4 shows that the VMS element exhibits latency in tracking the species front in time, but Figure 6 suggests that the overall concentration, or the integral of c over the domain is preserved. There is only a marginal difference between the two elements in predicting the time at which a steady state solution is reached. Also, both elements capture a smooth variation of concentration along the front, even though the VMS velocity field is not smooth.

Figure 7 shows the degree to which the VMS element violates local mass balance for problems of this nature. (A similar figure is not presented for the RT0 element because it is locally conservative to machine precision.) The error was calculated as $\text{div}[\mathbf{v}]$ over each element. Notice that the error is concentrated along the inflow and outflow boundaries. This is due to the well-known implications of imposing the pressure boundary conditions in weak fashion.

Remark 3. *Due to the well-known instabilities associated with a high ratio of advection to diffusion in the transport model [32, 33], some diffusion was necessary to include for numerical reasons, even though the primary quantities of interest are related to pure advection. Also a constant scalar diffusivity was chosen to avoid instabilities associated with violations of the discrete maximum-minimum principle [34, 35, 36].*

TABLE 2. Multilayer problem: parameters

Parameter	Value
ρ	996.1 kg/m ²
k_1	1×10^{-13} m ²
k_2	5×10^{-13} m ²
k_3	0.5×10^{-13} m ²
k_4	3×10^{-13} m ²
k_5	8×10^{-13} m ²
μ	1×10^{-8} kg/m-s
\mathbf{g}	(0,0,0)
p_o	1×10^5 Pa
Nodes	441
Elements	800

4.2. Cylinder inclusion problem. The cylinder inclusion problem can be conceptualized as a contaminant initially contained in a highly permeable porous media, encapsulated in a lower permeability media, that is dispersed by a cross-flow in the domain generated by a pressure drop. This problem is an adaptation from the problem presented in [37]. The primary quantity of interest in this problem is the degree to which the contaminant infiltrates the domain and the time scale of this process. The geometry of this problem is shown in Figure 8 along with the computational mesh. The permeability of the infinite domain, and other parameters is given Table 3.

Figure 9 shows the velocity magnitude for both elements. For the RT0 element, a smooth transition occurs from the highly permeable region to the region of lower permeability. On the other hand, the VMS element shows oscillations along the boundary of the two regions. Again, this is due to the continuity of the solution in the direction transverse to the interface for the VMS element. Figures 10 and 11 show the pressure and velocity along different portions of the domain. The overshoot of the velocity magnitude for the VMS element is also evident in these figures.

Figure 12 shows the concentration of the species in time as it deviates from the initial conditions. Both the RT0 and VMS elements again show tremendous similarity in the contours of concentration with respect to time. The local mass balance error for the VMS formulation is shown in Figure 13. Unlike in the multilayer problem, for the cylinder inclusion, the error is concentrated along the boundary of the inclusion, in particular where the interface is oriented tangentially to the flow direction. To more fully understand if these features are related to the magnitude of the jump in permeability, several cases were run in which the permeability of the inclusion was varied from 1×10^{-11} to 1×10^{-3} m². Figure 14 shows the error in the concentration for both elements as the

jump increases. As expected, the RT0 element performs well regardless of the jump in permeability, but even the VMS shows only a marginal error (less than 2%) even for the worst case scenario.

TABLE 3. Cylinder inclusion problem: parameters

Parameter	Value
ρ	996.1 kg/m ³
k_1	1×10^{-8} m ²
k_2	varies 1×10^{-11} to 1×10^{-3} m ²
μ	1.13×10^{-3} kg/m-s
\mathbf{g}	(0,0,0)
p_o	2.1721×10^5 Pa
Nodes	489
Elements	912

4.3. Leaky well problem. The leaky well problem represents the transport of a species as it is injected into an aquifer that contains an abandoned well that allows some of the species to escape. The primary quantity of interest is the rate at which the species escapes from the aquifer through the leak. This problem has been studied by a number of authors in evaluating subsurface modeling codes (see [38, 39, 5]) and is therefore important to study from the perspective of element choice, since the element choice could have a significant effect on the results. The domain is shown in Figure 15 along with the computational mesh.

The steady state pressure and velocity contours are shown in Figures 16 and 17. Given the velocity field computed by either element, the transport problem is solved by prescribing a Dirichlet boundary condition of $c = 1.0$ at the inflow. Thus, the injection rate is $\int cv_y dA_i$ and the leak rate is $\int cv_y dA_o$, where A_i is the area of the injection port and A_o is the area of the leaky well, both with diameter 0.3 m. For the leak rate, c is measured at the opening of the leaky well into Aquifer A. Figures 18 and 19 show similar results for the overall contours of concentration for results obtained using the Darcy flow model given in equation (1a).

Figure 20 shows the leak rate for various values of β from 0.0 to 1×10^{-9} using the Barus model given in equation (1b). Figure 20 shows that the dependence of the viscosity on the pressure has a strong influence on the predicted leak rate. This trend is also apparent in Figure 21, which shows contours of the concentration at time $t = 0.12$ days for various values of β . Notice the greater degree of penetration for the low values of β vs. high. The pressure dependent viscosity leads to both a lower leak rate and a longer time to steady-state conditions. Figure 20 reveals that the leak rate is substantially under-predicted by the VMS element. Although both elements predict

that the leak rate will reach a steady-state around $t = 2$ days for the case of $\beta = 0.0$, the VMS element shows a considerable decrease in the steady-state leak rate. Whereas for the previous two problems, the RT0 and VMS element performed remarkably similar, in this case the VMS element shows considerable variation. The results suggest that the VMS element is not an appropriate choice for this type of problem since it not only shows a significant accuracy error, but also an under-prediction of the quantity of interest which, from a design standpoint, is less conservative.

TABLE 4. Leaky well problem: parameters

Parameter	Value
ρ	479 kg/m ²
k_1	1×10^{-12} m ²
k_2	1×10^{-14} m ²
μ_0	3.95×10^{-5} kg/m-s
\mathbf{g}	(0,0,-9.8) m/s ²
Injection pressure	2.03×10^9 Pa
Open boundary pressure	$3.075 \times 10^7 + 1.025 \times 10^4(\text{depth})$ Pa
Nodes	23126
Elements	43098

4.4. Computational efficiency. In this section, we evaluate both elements from the perspective of computation time and memory usage. The most significant drawback pointed out for the RT0 element is that it is not scalable as the problem size grows. This is due to the RT0 element formulation having variables that exist on the element edges, which in turn leads to more equations in the linear system. Simply put, a node unknown can be shared by many elements, where as an edge or face unknown can be shared by only two elements. The fewer elements that can share an unknown, the larger the system. Although the problems shown in this work are only two dimensional, effects of this drawback are present. Table 5 shows the number of unknowns, assembly time, solve time, and memory usage of both elements for all of the examples above. Note that for each problem the number of unknowns is substantially higher for the RT0 element, roughly 30%. If this were the only consideration, the VMS element would be the clear winner, but taking into account the computation time as well, the VMS element takes substantially longer to assemble and solve the linear system. This is due to the additional stabilization terms that must be computed at each step. As expected, the time savings decrease as the problem size increases since at some point the problem size offsets the faster computation for the RT0 element.

The same is true for the memory usage. For the two smaller problems, the memory usage is identical, but for the leaky well problem, the VMS element requires less memory. The results suggest that for small to moderately sized problems (less than 100,000 degrees of freedom) the RT0 element is more efficient, but for large problems the VMS element is more efficient.

TABLE 5. Timing and memory usage data

Quantity	Multilayer		Cylinder Inclusion		Leaky well	
	RT0	VMS	RT0	VMS	RT0	VMS
Total unknowns	2481	1764	2801	1956	132447	92504
Assembly time/time step (s)	0.0323	0.05162	0.0345	0.05746	2.943	4.246
System solve/time step (s)	0.0327	0.04056	0.0156	0.04959	2.564	2.320
Required memory storage (MB)	233	233	227	227	421	396
Problem size savings	–	28.9%	–	30.1%	–	30.2%
Time savings	29.5%	–	53.2%	–	16.1%	–
Memory savings	–	–	–	–	–	5.9%

5. CONCLUSIONS

The results of this study reveal several interesting features of the lowest Raviart-Thomas and the variational multiscale formulation when used to model flow through heterogeneous porous media. Although the equal-order interpolation for the velocity and pressure under the variational multiscale formulation does not exhibit local (or element) mass balance. In addition, the formulation also shows oscillations in the velocity field when the primary flow direction is tangential to jumps in permeability, for some transport problems, the resulting concentration field is only marginally affected. For the multilayer problem and the cylinder inclusion problem, the mass conservation error produced by using the variational multiscale formulation is less than 2%. On the other hand, for transport problems similar to the leaky well problem, the equal-order interpolation under the variational multiscale formulation not only shows a substantial error in the concentration, but also under-predicts the leak rate, which is undesirable from a design perspective. For the leaky well problem, the leak rate was under-predicted by roughly 10% by the variational multiscale formulation. The results of this study also reveal that for small to moderately sized problems, the increased size of the linear system of equations for the RT0 formulation is offset by a reduced computation time. For large problems, this advantage diminishes. In general, these results give some perspective on the computational cost associated with using a locally mass conserving element, and the accuracy cost of using a stabilized element.

ACKNOWLEDGMENTS

This work was supported in part (D. Z. Turner and P. K. Notz) by the Laboratory Directed Research and Development program at Sandia National Laboratories. Sandia is a multiprogram laboratory operated by Sandia Corporation, a Lockheed Martin Company, for the United States Department of Energy's National Nuclear Security Administration under Contract DE-AC04-94AL85000. The research reported herein was also supported (K. B. Nakshatrala) by the Texas Engineering Experiment Station (TEES). This support is gratefully acknowledged. The opinions expressed in this paper are those of the authors and do not necessarily reflect that of the sponsors. The authors would like to thank Mario Martinez for many useful discussions on this topic.

REFERENCES

- [1] P. A. Raviart and J. M. Thomas. A mixed finite element method for 2nd order elliptic problems. In *Mathematical Aspects of the Finite Element Method*, pages 292–315, Springer-Verlag, New York, 1977.
- [2] K. B. Nakshatrala, D. Z. Turner, K. D. Hjelmstad, and A. Masud. A stabilized mixed finite element method for Darcy flow based on a multiscale decomposition of the solution. *Computer Methods in Applied Mechanics and Engineering*, 195(33-36):4036–4049, 2006.
- [3] A. Masud and T. J. R. Hughes. A stabilized mixed finite element method for Darcy flow. *Computer Methods in Applied Mechanics and Engineering*, 191:4341–4370, 2002.
- [4] K. B. Nakshatrala and K. R. Rajagopal. A numerical study of fluids with pressure dependent viscosity flowing through a rigid porous medium. *International Journal for Numerical Methods in Fluids*, DOI: 10.1002/flid.2358, 2010.
- [5] K. B. Nakshatrala and D. Z. Turner. A stabilized mixed formulation for modified Darcy equation. *International Journal of Engineering Science*, DOI: 10.1016/j.ijengsci.20010.08.009, 2010.
- [6] F. Brezzi and M. Fortin. *Mixed and Hybrid Finite Element Methods*, volume 15 of Springer Series in Computational Mathematics. Springer-Verlag, New York, USA, 1997.
- [7] F. Brezzi, J. Douglas, and L. D. Marini. Two families of mixed elements for second order elliptic problems. *Numerische Mathematik*, 88:217–235, 1985.
- [8] G. R. Barrenechea, L. P. Franca, and F. Valentin. A Petrov-Galerkin enriched method: A mass conservative finite element method for the Darcy equation. *Computer Methods in Applied Mechanics and Engineering*, 196:2449–246, 2007.
- [9] T. Arbogast, Y. Huang, and T. F. Russel. A locally conservative streamline method for a model two-phase flow problem in a one-dimensional porous medium. *Submitted*. <http://users.ices.utexas.edu/arbogast/PaperArchive/paperIndex.html>, 2010.
- [10] A. Mazzia, G. Pini, M. Putti, and F. Sarteretto. Comparison of 3D flow fields arising in mixed and standard unstructured finite elements. *Lecture Notes in Computer Science: Part I*, pages 560–567, 2003.
- [11] V. Kippe, J. E. Aarnes, and K. Lie. Multiscale finite-element methods for elliptic problems in porous media flow. *Proceedings of CMWR XVI - Computational Methods in Water Resources, Copenhagen, Denmark*, June 2006.
- [12] L. J. Durlofsky. Accuracy of mixed and control volume finite element approximations to Darcy velocity and related quantities. *Water Resources Research*, 30:965–973, 1994.

- [13] T. J. R. Hughes, G. Engel, L. Mazzei, and M. G. Larson. The continuous Galerkin method is locally conservative. *Journal of Computational Physics*, 163:467–488, 2000.
- [14] E. C. Dogrul and T. N. Kadir. Flow computation and mass balance in Galerkin finite-element groundwater models. *Journal of Hydraulic Engineering*, 132:1206–1214, 2006.
- [15] H. Darcy. Les Fontaines Publiques de la Ville de Dijon. *Victor Dalmont, Paris*, 1856.
- [16] C. Barus. Isotherms, isopiestic and isometrics relative to viscosity. *American Journal of Science*, 45:87–96, 1893.
- [17] L. C. Evans. *Partial Differential Equations*. American Mathematical Society, Providence, Rhode Island, USA, 1998.
- [18] F. Brezzi and M. Fortin. *Mixed and Hybrid Finite Element Methods, volume 15 of Springer series in computational mathematics*. Springer-Verlag, New York, USA, 1991.
- [19] O. A. Ladyzhenskaya. *The Boundary Value Problems of Mathematical Physics*. Springer-Verlag, New York, USA, 1985.
- [20] I. Babuška. Error bounds for finite element methods. *Numerische Mathematik*, 16:322–333, 1971.
- [21] L. P. Franca and T. J. R. Hughes. Two classes of mixed finite element methods. *Computer Methods in Applied Mechanics and Engineering*, 69:89–129, 1988.
- [22] A. Masud and T. J. R. Hughes. A stabilized mixed finite element method for Darcy flow. *Computer Methods in Applied Mechanics and Engineering*, 191:4341–4370, 2002.
- [23] K. B. Nakshatrala, D. Z. Turner, K. D. Hjelmstad, and A. Masud. A stabilized mixed finite element formulation for Darcy flow based on a multiscale decomposition of the solution. *Computer Methods in Applied Mechanics and Engineering*, 195:4036–4049, 2006.
- [24] F. Brezzi, J. Douglas, and L. D. Marini. Two families of mixed elements for second order elliptic problems. *Numerische Mathematik*, 47:217–235, 1985.
- [25] M. S. Engelman, R. L. Sani, and P. M. Gresho. The implementation of normal and/or tangential boundary conditions in finite element codes for incompressible fluid flow. *International Journal for Numerical Methods in Fluids*, 2:225–238, 1982.
- [26] Y. Bazilevs and T. J. R. Hughes. Weak imposition of Dirichlet boundary conditions in fluid mechanics. *Computers & Fluids*, 36:12–26, 2007.
- [27] R. L. Sani, J. Shen, O. Pironneau, and P. M. Gresho. Pressure boundary condition for the time-dependent incompressible Navier-Stokes equations. *International Journal for Numerical Methods in Fluids*, 50:673–682, 2006.
- [28] R. L. Sani and P. M. Gresho. Resume and remarks on the open boundary condition minisymposium. *International Journal for Numerical Methods in Fluids*, 18:983–1008, 1994.
- [29] M. Sala, K. Stanley, and M. Heroux. Amesos: A set of general interfaces to sparse direct solver libraries. In *Proceedings of PARA'06 Conference, Umea, Sweden*, 2006.
- [30] J. Wan. Stabilized finite element methods for coupled geomechanics and multiphase flow. *PhD Dissertation, Stanford University*, 2002.
- [31] T. J. R. Hughes, A. Masud, and J. Wan. A stabilized mixed discontinuous Galerkin method for Darcy flow. *Computer Methods in Applied Mechanics and Engineering*, 195:3347–3381, 2006.
- [32] A. Masud and R. A. Khurram. A multiscale/stabilized finite element method for the advection-diffusion equation. *Computer Methods in Applied Mechanics and Engineering*, 193:1997–2018, 2004.

- [33] D. Z. Turner, K. B. Nakshatrala, and K. D. Hjelmstad. A stabilized formulation for the advection-diffusion equation using the generalized finite element method. *International Journal for Numerical Methods in Fluids*, DOI: 10.1002/fld.2248, 2010.
- [34] R. Liska and M. Shashkov. Enforcing the discrete maximum principle for linear finite element solutions for elliptic problems. *Communications in Computational Physics*, 3:852–877, 2008.
- [35] K. B. Nakshatrala and A. J. Valocchi. Non-negative mixed finite element formulations for a tensorial diffusion equation. *Journal of Computational Physics*, 228:6726–6752, 2009.
- [36] H. Nagarajan and K. B. Nakshatrala. Enforcing the non-negativity constraint and maximum principles for diffusion with decay on general computational grids. *International Journal for Numerical Methods in Fluids*, In print, DOI: 10.1002/fld.2389, 2010.
- [37] J. L. Gupta. Fluid motion past a porous circular cylinder with initial pressure gradient. *Journal of Applied Mechanics*, 47:489–492, 1980.
- [38] A. Ebigbo, H. Class, and R. Helmig. CO₂ leakage through an abandoned well: problem-oriented benchmarks. *Computers & Geoscience*, 11:103–115, 2007.
- [39] J. M. Nordbotten, M. A. Celia, S. Bachu, and H. K. Dahle. Semianalytical solution for CO₂ leakage through an abandoned well. *Environmental Science and Technology*, 39:602–611, 2005.

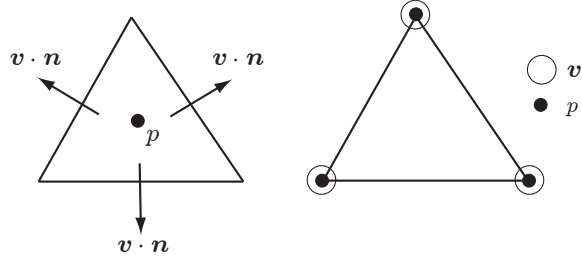


FIGURE 1. The left figure shows the degrees-of-freedom in the lowest-order Raviart-Thomas (RT0) formulation, and the right figure shows the degrees-of-freedom in the (equal-order) VMS formulation.

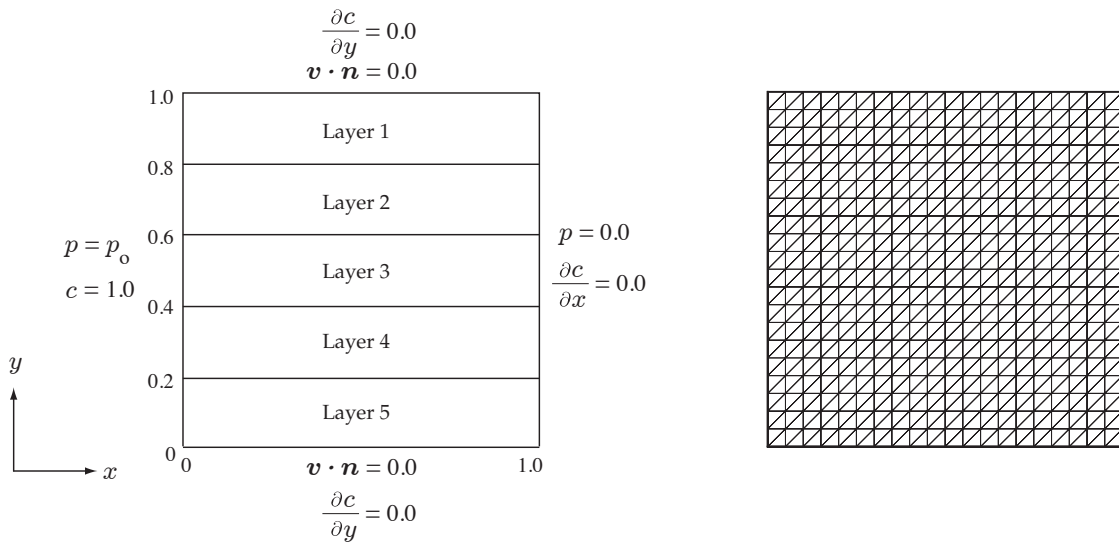


FIGURE 2. Multilayer problem: The left figure shows the geometry and boundary conditions, and the right figure shows the computational mesh employed in the numerical simulation.

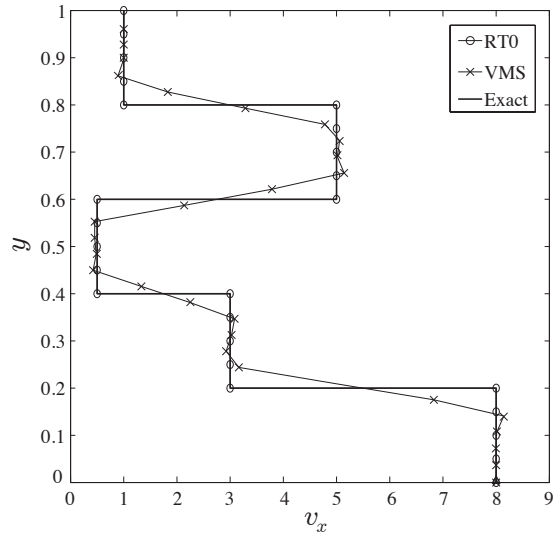


FIGURE 3. Multilayer problem: Variation of x -velocity along the vertical centerline of the domain at $x = 0.5$.

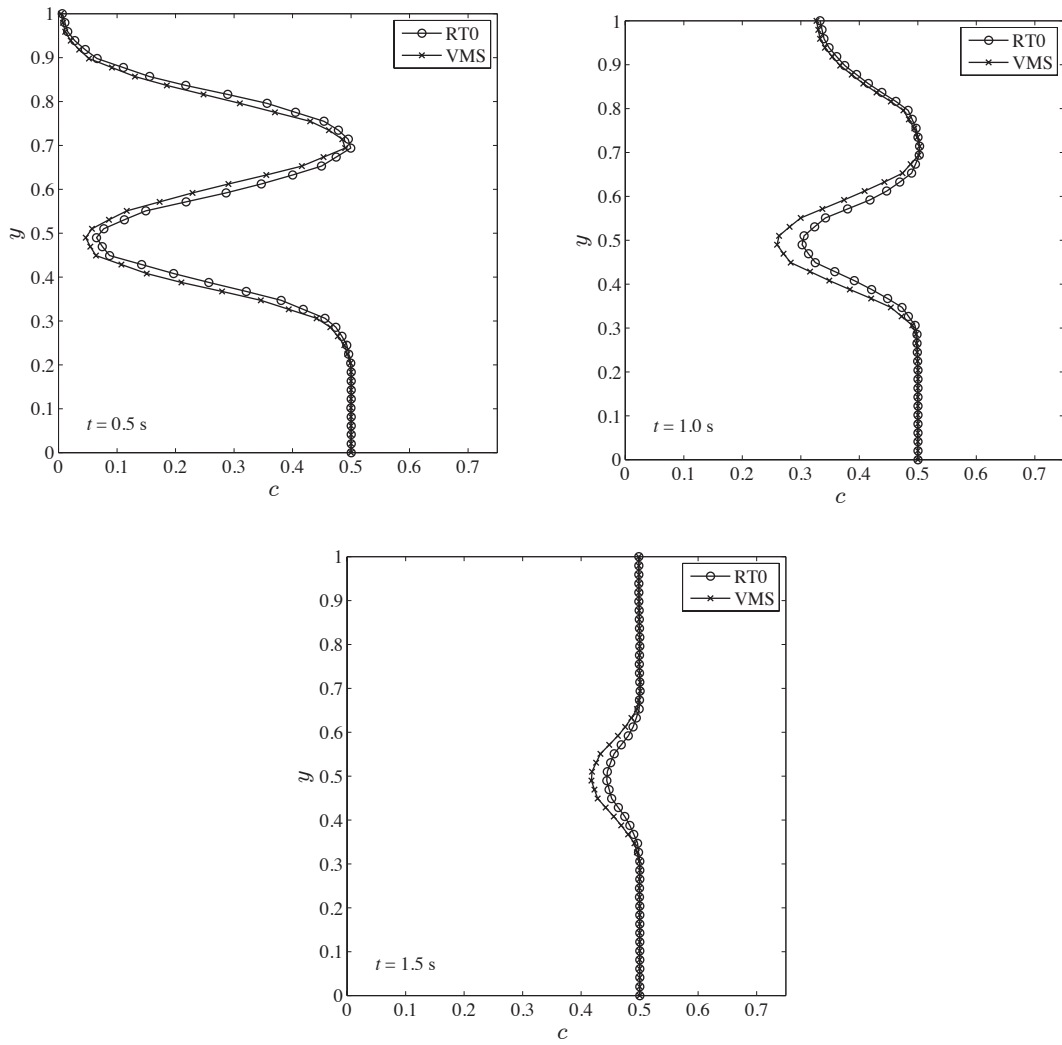


FIGURE 4. Multilayer problem: Variation of the concentration along the vertical line of the domain at $x = 1.0$ for various instances of time $t = 0.5, 1.0$ and 1.5 s.

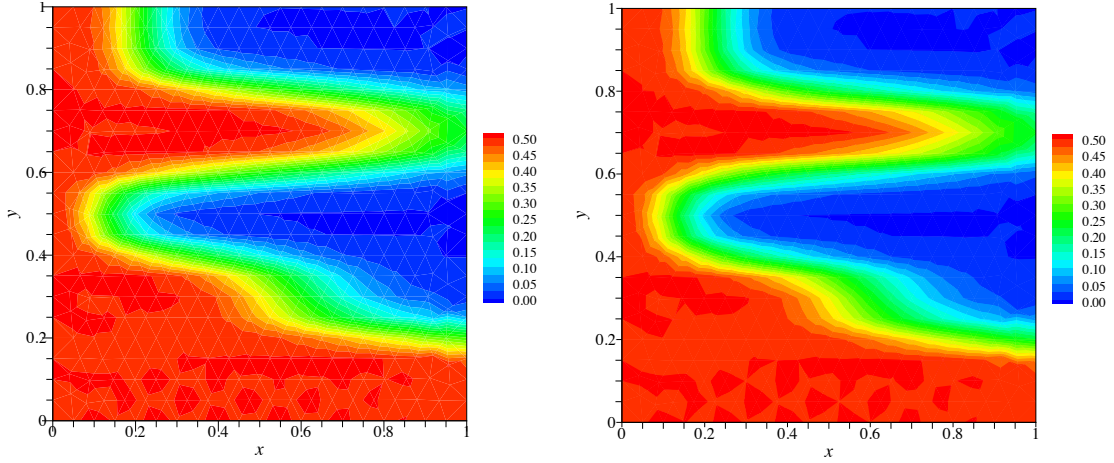


FIGURE 5. Multilayer problem: Contours of the concentration at time $t = 0.2$ s using the RT0 formulation (left) and the variational multiscale formulation (right).

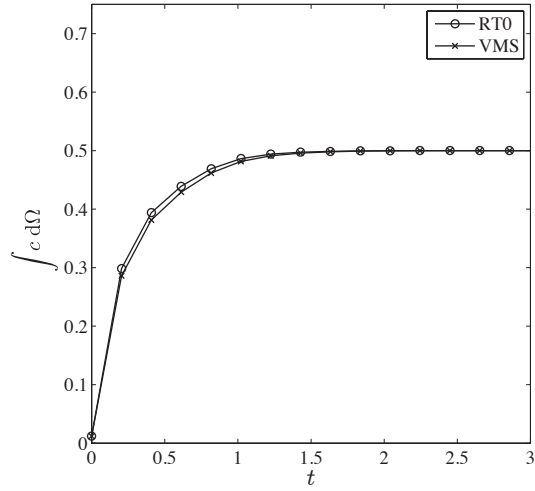


FIGURE 6. Multilayer problem: This figure shows the variation of the total concentration with time. The total concentration is the integral of the concentration field over the entire domain.

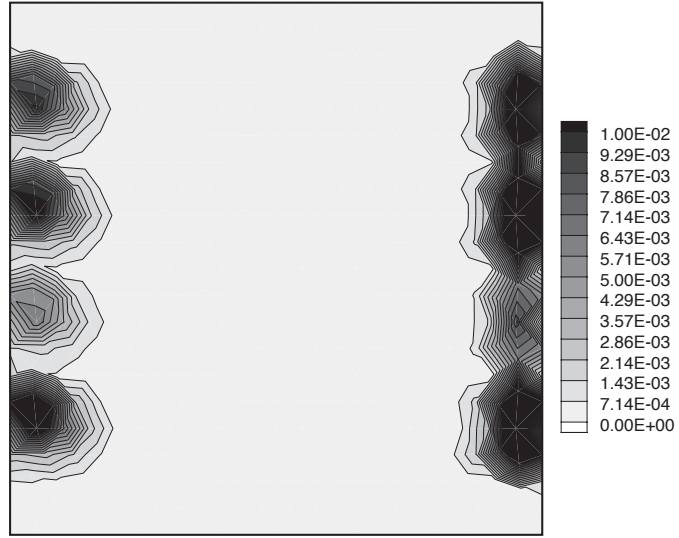


FIGURE 7. Multilayer problem: This figure shows the contours of the error in the local mass balance under the equal-order variational multiscale formulation.

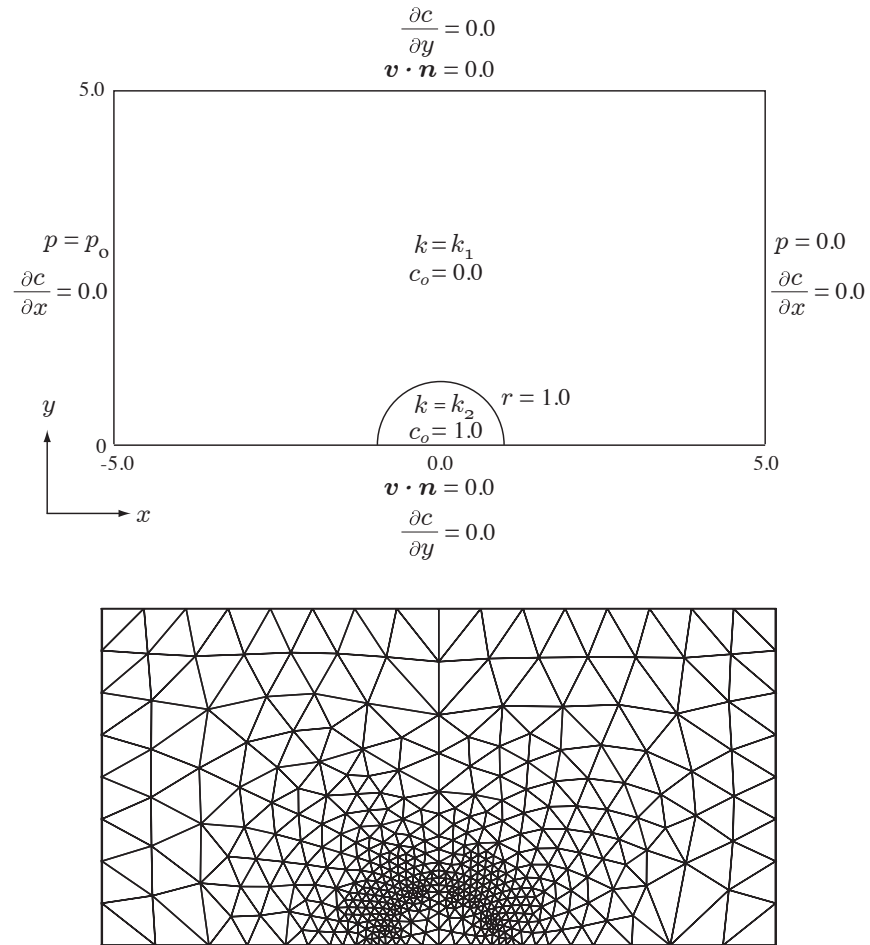


FIGURE 8. Cylinder inclusion: The top figure shows the problem geometry and boundary conditions, and the bottom figure shows the computational mesh used in the numerical simulation.

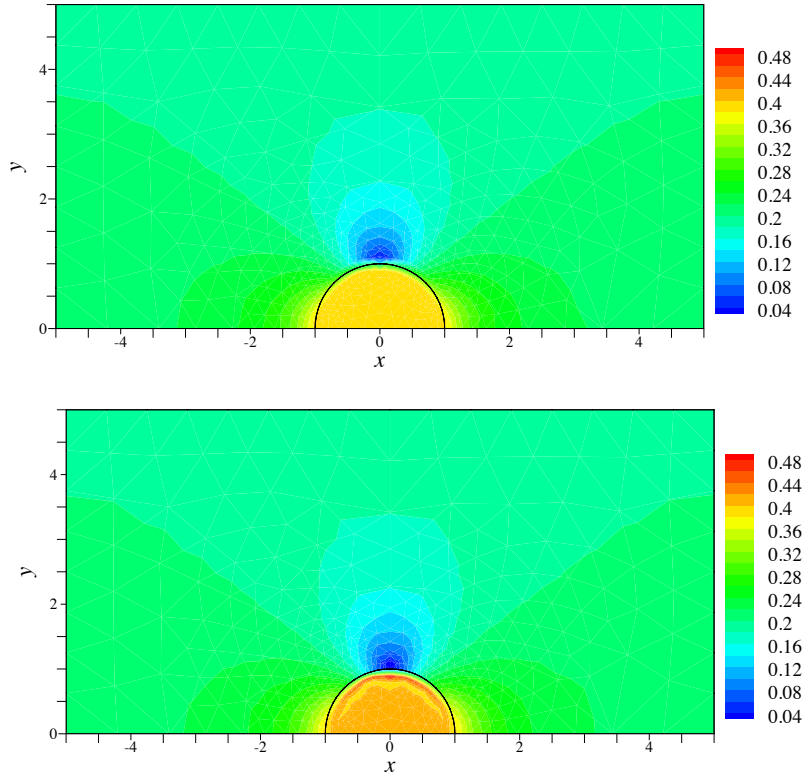


FIGURE 9. Cylinder inclusion: This figure shows the contours of the magnitude of the velocity using the RT0 formulation (top) and the variational multiscale formulation (bottom) for the case $k_2 = 1 \times 10^{-3}$.

DR. DANIEL Z. TURNER, COMPUTATIONAL THERMAL & FLUID MECHANICS DEPARTMENT, SANDIA NATIONAL LABORATORIES, MAIL STOP 0836, PO BOX 5800, ALBUQUERQUE, NEW MEXICO - 87185.

E-mail address: dzturnd@sandia.gov

PROFESSOR KALYANA BABU NAKSHATRALA, DEPARTMENT OF MECHANICAL ENGINEERING, 216 ENGINEERING/PHYSICS BUILDING, TEXAS A&M UNIVERSITY, COLLEGE STATION, TEXAS - 77843. TEL:+1-979-845-1292

E-mail address: knakshatrala@tamu.edu

DR. PATRICK K. NOTZ, COMPUTATIONAL THERMAL & FLUID MECHANICS DEPARTMENT, SANDIA NATIONAL LABORATORIES, MAIL STOP 0836, PO BOX 5800, ALBUQUERQUE, NEW MEXICO - 87185.

E-mail address: pknotz@sandia.gov

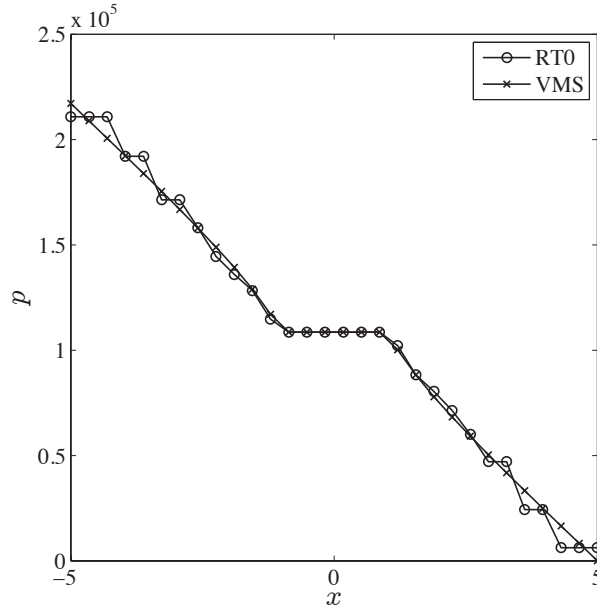


FIGURE 10. Cylinder inclusion: This figure shows the variation of the pressure along x -direction at $y = 0$ for the case $k_2 = 1 \times 10^{-3}$.

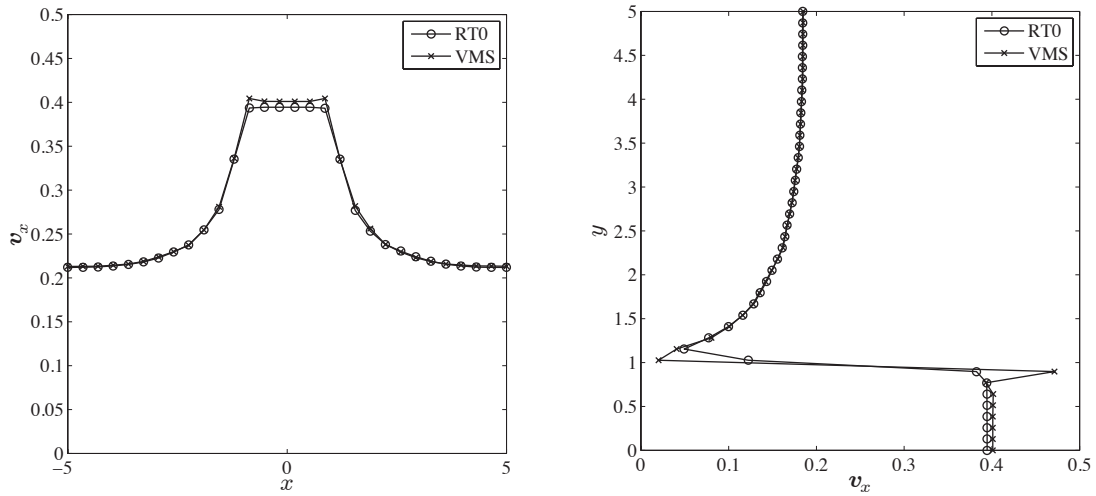


FIGURE 11. Cylinder inclusion: This figure shows the variation of the x -velocity along the x -direction at $y = 0$ (left), and along the y -direction at $x = 0$ (right) for the case $k_2 = 1 \times 10^{-3}$.

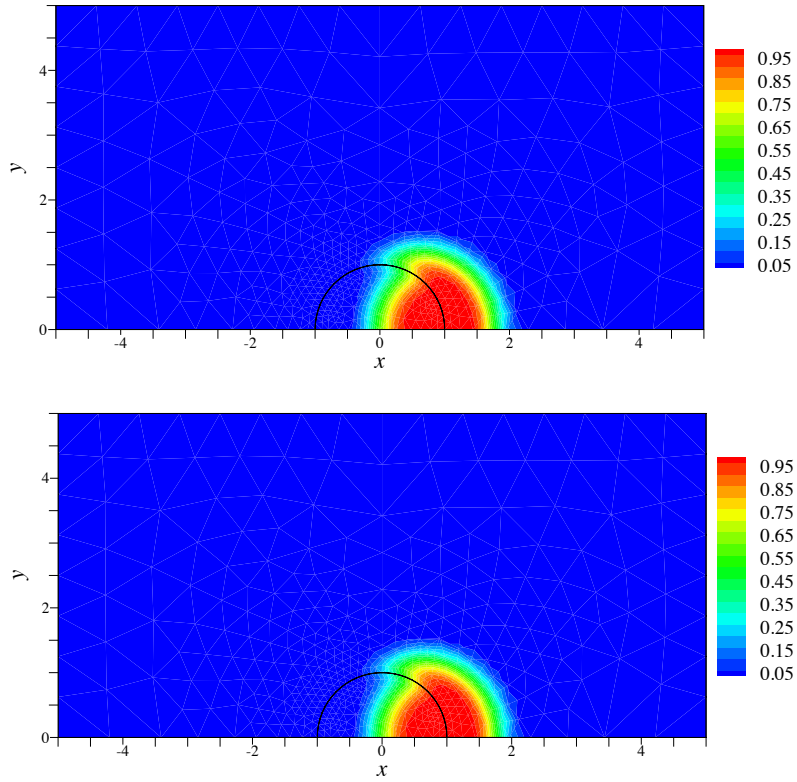


FIGURE 12. Cylinder inclusion: This figure shows the contours of the concentration at time $t = 1.5$ s using the RT0 formulation (top) and the variational multiscale formulation (bottom) for the case $k_2 = 1 \times 10^{-3}$.

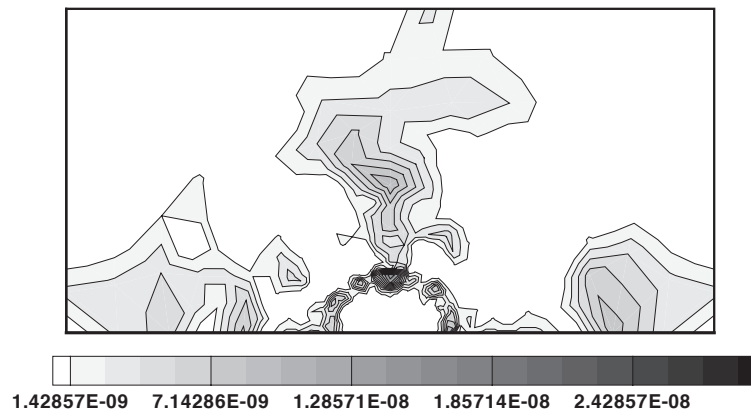


FIGURE 13. Cylinder inclusion: This figure shows the contours of the error in the mass balance using the variational multiscale formulation for the case $k_2 = 1 \times 10^{-7}$.

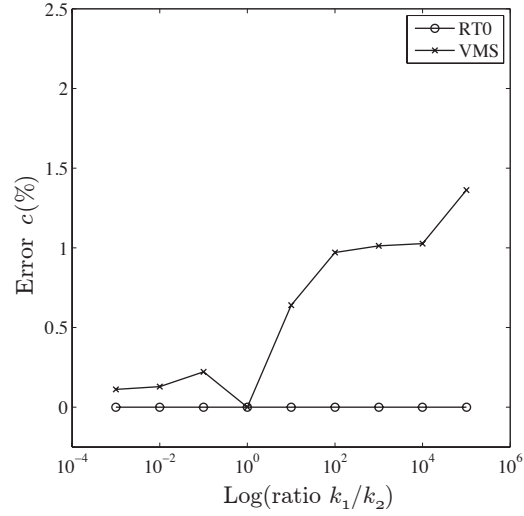


FIGURE 14. Cylinder inclusion: The figure shows the variation of the error in the total concentration (which is measured as the difference between the integral of c over the domain at time $t = 2.5$ s minus the integral of c over the domain at $t = 0.0$ s) with respect to the log of the ratio of permeabilities between the inclusion and the rest of the domain.

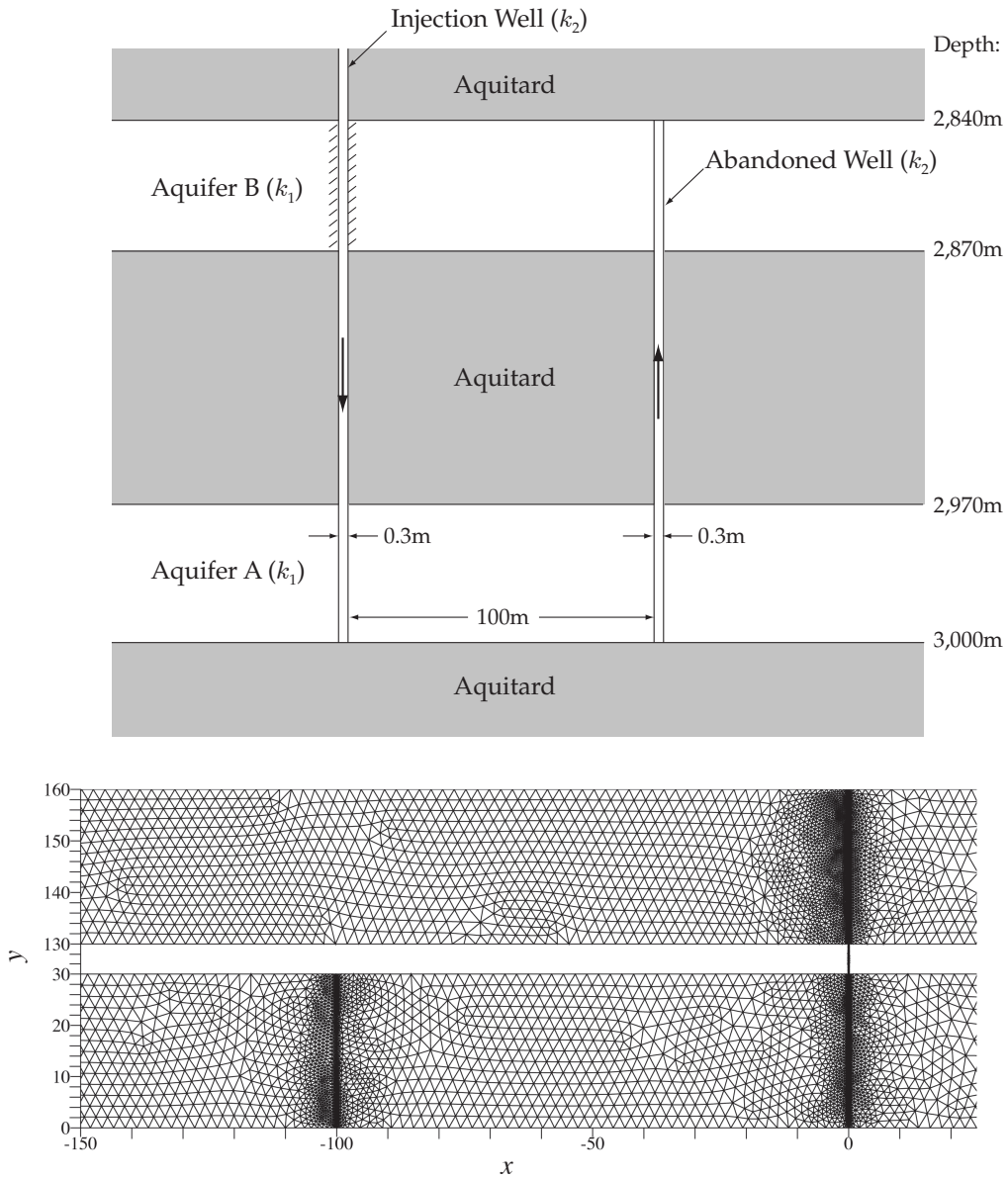


FIGURE 15. Leaky well: A pictorial description of the problem (top) and the computational mesh used in the numerical simulation (bottom). (Note that a portion of the mesh for the abandoned well is omitted to facilitate plotting.)

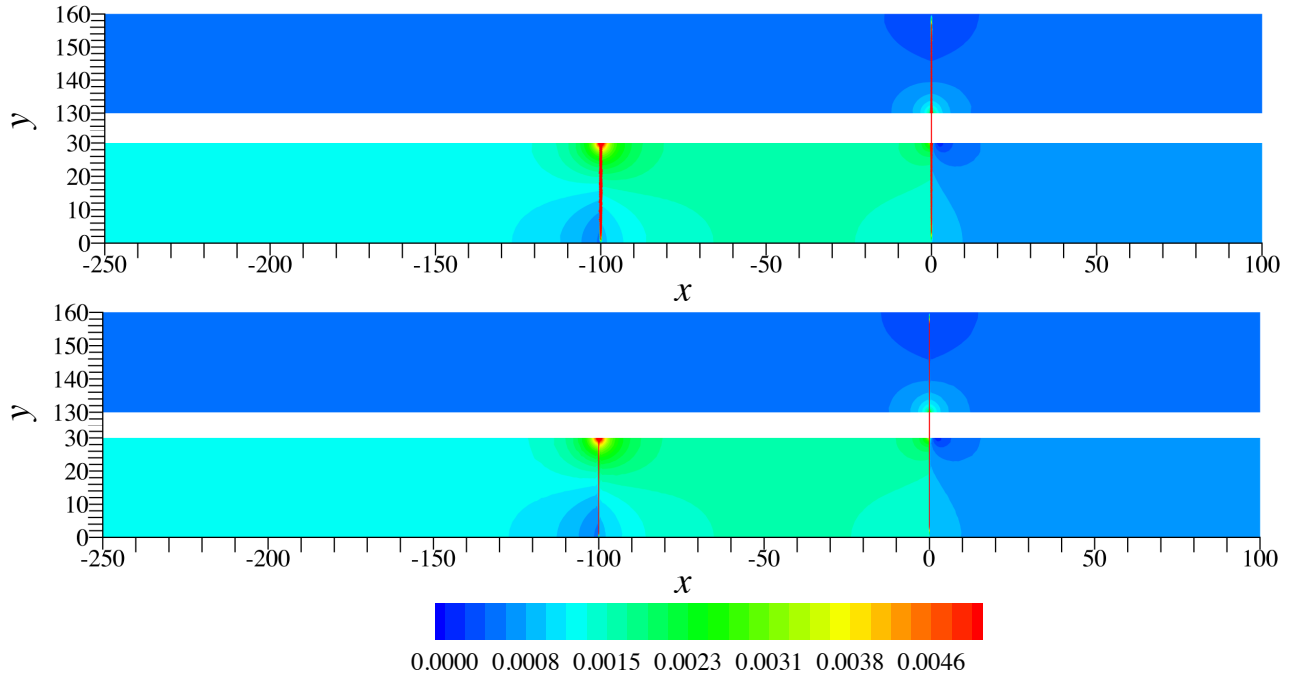


FIGURE 16. Leaky well: velocity magnitude contours using the RT0 formulation (top) and the variational multiscale formulation (bottom).

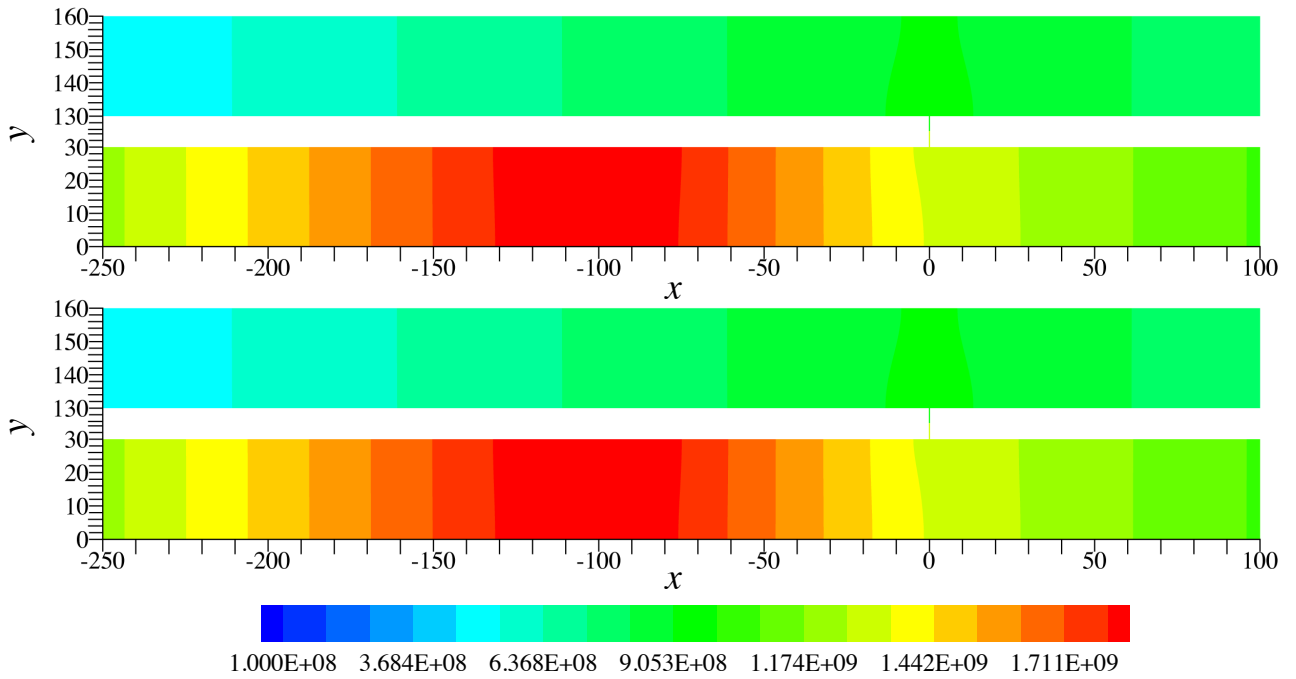


FIGURE 17. Leaky well: pressure contours using the RT0 formulation (top) and the variational multiscale formulation (bottom).

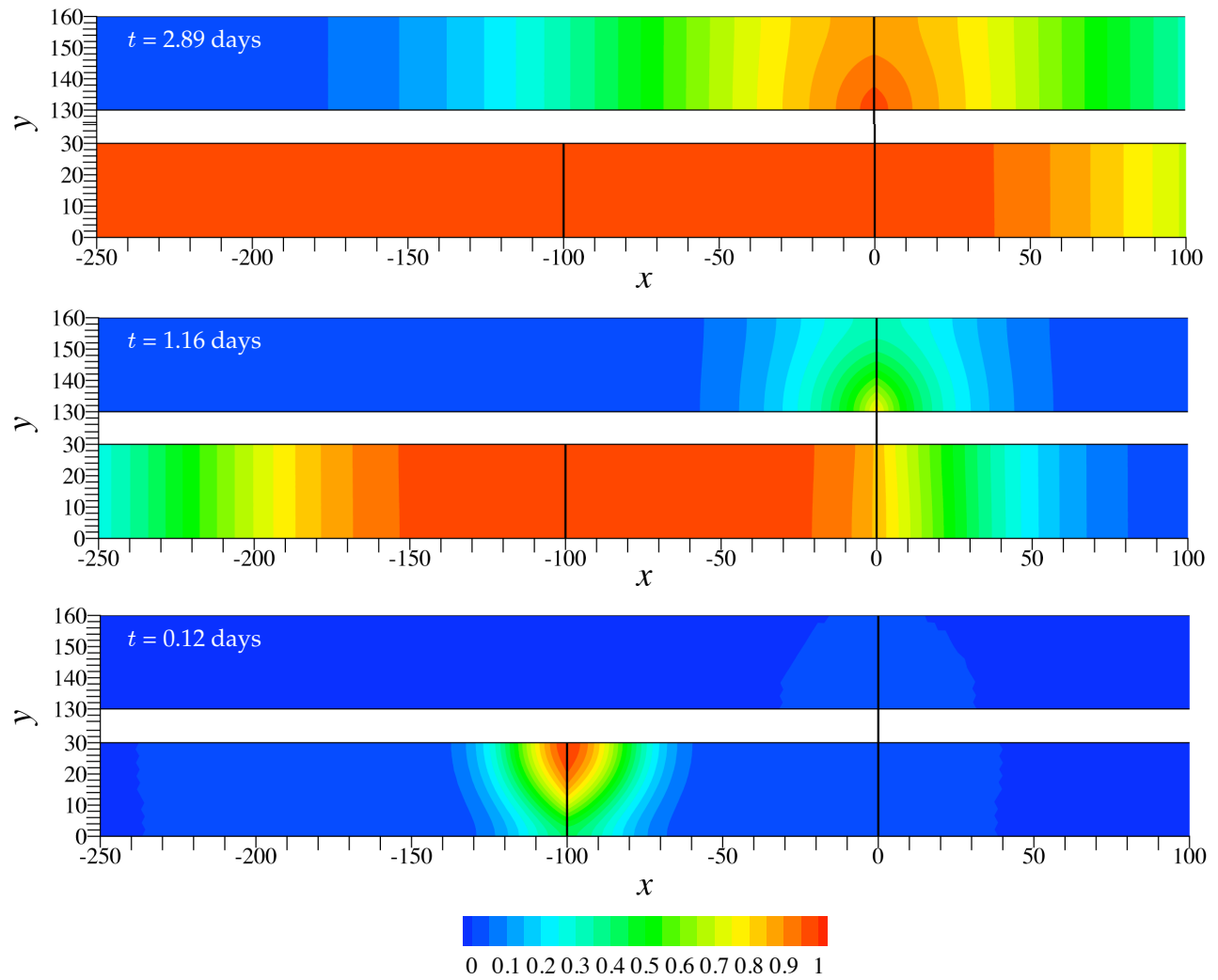


FIGURE 18. Leaky well: contours of concentration at various times for the RT0 formulation. (Note that a portion of the abandoned well was omitted to facilitate plotting.)

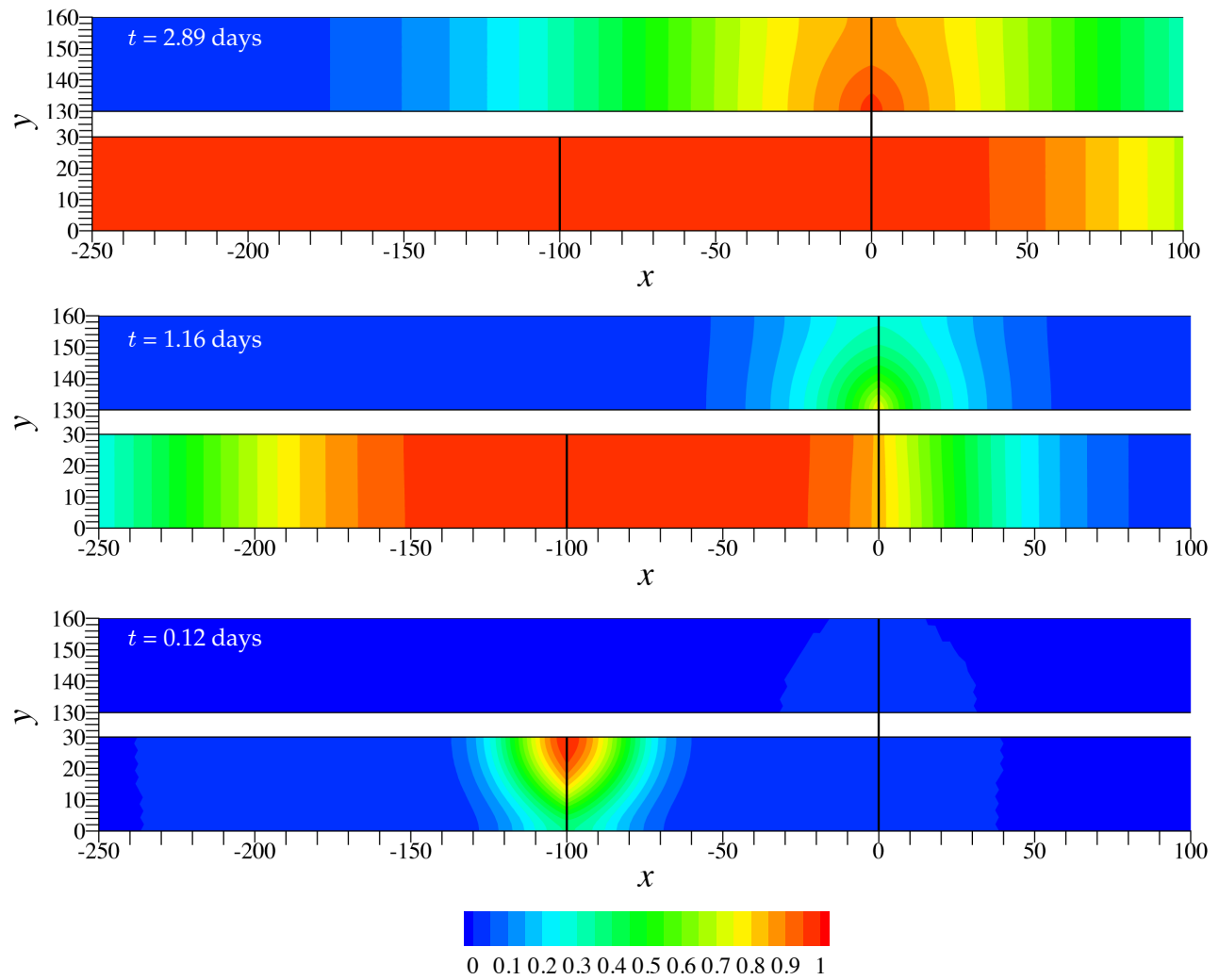


FIGURE 19. Leaky well: contours of concentration at various instances of time for the variational multiscale formulation. (Note that a portion of the abandoned well was omitted to facilitate plotting.)

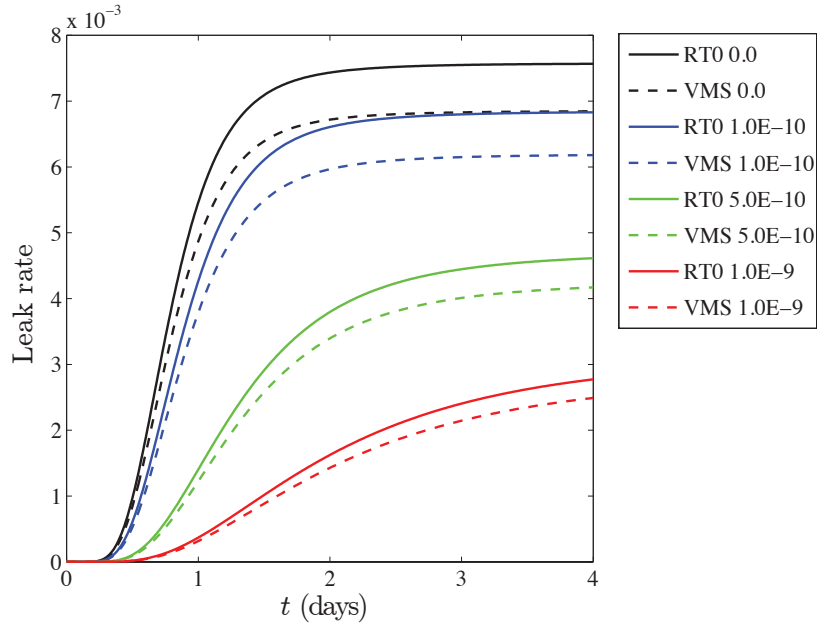


FIGURE 20. Leaky well: leak rate vs. time measured as the concentration times the mass flux across the opening of the abandoned well into Aquifer B for various values of β using the Barus model for viscosity given in equation (1b).

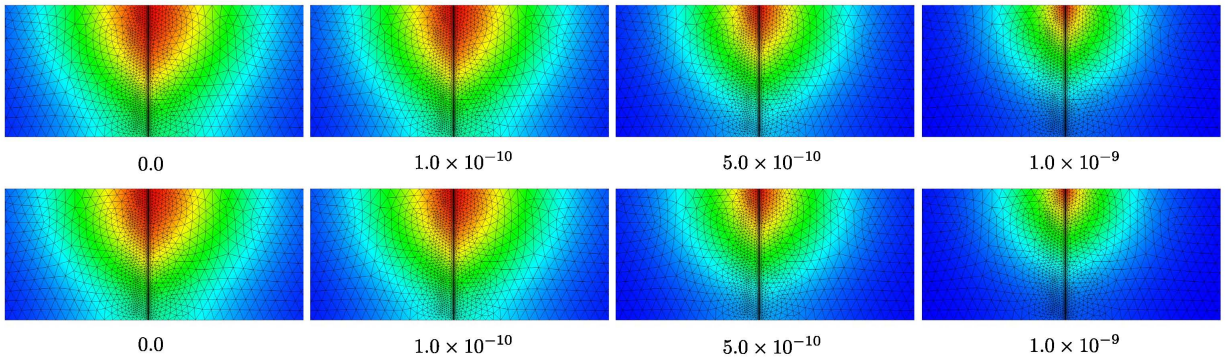


FIGURE 21. Leaky well: contours of the concentration at the injection well at $t = 0.12$ days for various values of β using the Barus model for viscosity given in equation (1b) (top) RT0 (bottom) VMS.